

Test Beam Studies Of Silicon Timing for Use in Calorimetry.

A. Apresyan¹, G. Bolla², A. Bornheim¹, H. Kim³, S. Los², C. Pena¹, E. Ramberg²,
A. Ronzhin², M. Spiropulu¹, and S. Xie¹

¹*California Institute of Technology, Pasadena, CA, USA*

²*Fermi National Accelerator Laboratory, Batavia, IL, USA*

³*University of Chicago, Chicago, IL, USA*

Abstract

The high luminosity upgrade of the Large Hadron Collider (HL-LHC) at CERN is expected to provide instantaneous luminosities of $5 \times 10^{34} \text{ cm}^{-2} \text{ s}^{-1}$. The high luminosities expected at the HL-LHC will be accompanied by a factor of 5 to 10 more pileup compared with LHC conditions in 2015, causing general confusion for particle identification and event reconstruction. Precision timing allows to extend calorimetric measurements into such a high density environment by subtracting the energy deposits from pileup interactions. Calorimeters employing silicon as the active component have recently become a popular choice for the HL-LHC and future collider experiments which face very high radiation environments. In this article, we present studies of basic calorimetric and precision timing measurements using a prototype composed of tungsten absorber and silicon sensor as the active medium. We show that for the bulk of electromagnetic showers induced by electrons in the range of 20 GeV to 30 GeV, we can achieve time resolutions better than 25 ps per single pad sensor.

1 Introduction

Future colliders, including the high luminosity upgrade of the Large Hadron Collider (HL-LHC) at CERN, will require improvements to the instantaneous luminosity by an order of magnitude or more compared to what has been achieved at the LHC so far. With the increased instantaneous luminosity the rate of simultaneous interactions per bunch crossing (pileup) is projected to reach an average of 140 to 200. The large amount of pileup increases the likelihood of confusion in the reconstruction of events of interest, due to the contamination from particles produced in different pileup interactions. The ability to discriminate between jets produced in the events of interests, especially those associated with the vector boson fusion processes, and jets produced by pileup interactions will be degraded. The missing transverse energy resolution will deteriorate, and several other physics object performance metrics will suffer.

One way to mitigate the pileup confusion effects, complementary to precision tracking methods, is to perform a time of arrival measurement associated with a particular layer of the calorimeter, allowing for a time assignment for charged particles and photons. Such a measurement with a precision of about 20-30 ps, when unambiguously associated to the corresponding energy measurement, will reduce the effective amount of pileup by a factor of 10, given that the spread in collision time of the pileup interactions at HL-LHC is foreseen to be approximately 200 ps. The association of the time measurement with the energy measurement is crucial, and leads to a prototype design that calls for the time and energy measurements to be performed in the same detector element. Since both the energy and time measurement are performed in the same detector element, once

an energy deposit is identified as originating from a pileup interaction, it can be unambiguously removed from event reconstruction.

Several alternative options to combine high resolution energy and timing measurements for calorimetry have been reported in Refs. [1–5]. In this article, we describe the continuation of this program of study using a calorimeter prototype employing a silicon pad sensor of $6 \times 6 \text{ mm}^2$ size as the active element. Silicon-based calorimeters have recently become a popular choice for future colliders due to the radiation hardness of silicon, and the ability to construct highly granular detectors. An important example is the forward calorimeter proposed for the CMS Phase 2 Upgrade [6]. We study the timing properties of silicon-based calorimetry using a prototype composed of tungsten absorber and a silicon sensor produced by Hamamatsu [7].

The paper is organized as follows. General silicon timing properties and bench test results are described in Section 2. The test beam setup and experimental apparatus are presented in Section 3. The results of the test beam measurements are presented in Section 4. Sections 5 and 6 are devoted to discussion and conclusion, respectively.

2 General Properties of Silicon Timing and Bench Test Studies

For our measurements, we used a silicon sensor produced by Hamamatsu [7]. The thickness of the silicon was measured to be $325 \mu\text{m}$. The transverse size of the sensor is $6 \times 6 \text{ mm}^2$. The negative bias voltage was applied to the p-side of the silicon. The capacitance of the silicon diode is measured as a function of the bias voltage and shown in Figure 1. We observe that the silicon is fully depleted above about 120 V. Timing measurements are expected to improve with larger bias voltage as the carrier velocity increases.

The electric diagram of the silicon diode connections is presented in Figure 2. Attention was paid to provide good filtering for bias voltage, to reduce ground loop effects, and to minimize inductive loop for the signal readout. The timing characteristics of the signal pulses are dominated primarily by properties of the silicon sensor rather than the details of the circuit.

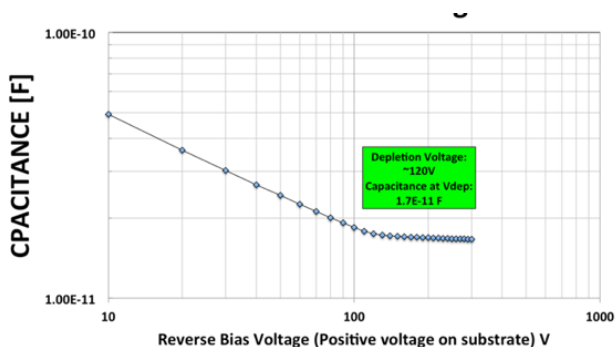


Figure 1: The measured capacitance as a function of the applied bias voltage.

The silicon diode was placed inside a light-tight box of thickness 1.5 cm, which also provides electromagnetic shielding. The box is made of 0.2 mm steel. The bias voltage was supplied to the circuitry by a cable with a balun filter, terminated with an SHV connector. The silicon diode output signal is read out through an SMA connector electrically grounded to the box. The dark current was measured at several values of the bias voltage. The maximum value of the dark current was less than 1.0 nA at -500 V , which is the largest bias voltage used in the measurements reported in this paper. The silicon box and bench test setup are presented in Figure 2.

The signals from the silicon sensor were amplified by two fast, high-bandwidth pre-amplifiers connected in series. The first amplifier is an ORTEC VT120C pre-amplifier, and the second amplifier is a Hamamatsu C5595 amplifier. Using a pulse-generator, we measured the combined gain

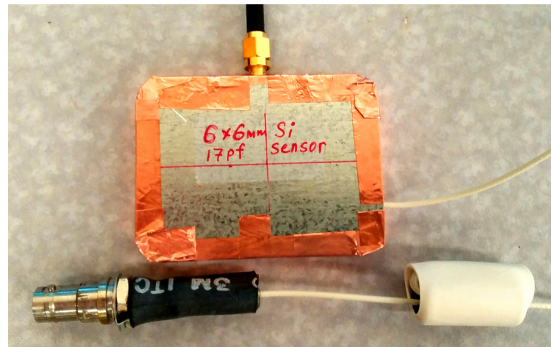
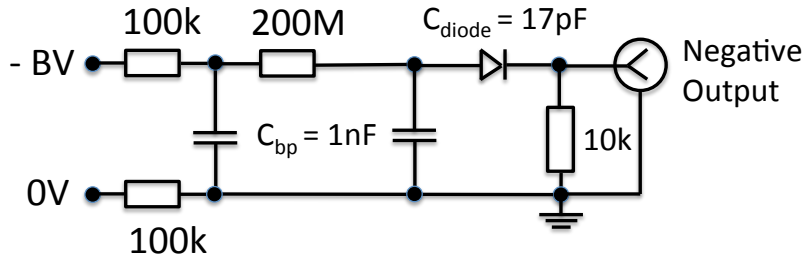


Figure 2: The electric diagram for the silicon diode connections (left). External view of the box with silicon diode, and the bias voltage connection is shown below it (right).

of the two amplifiers in series as a function of the input signal amplitude and found some degree of non-linearity for typical signals produced by the silicon sensor under study. The measured gain ranged from 200 for signals with amplitude around 0.15 mV to 650 for signals with amplitude around 10 mV.

3 Test-beam Setup and Experimental Apparatus

We performed the test-beam measurements at the Fermilab Test-beam Facility (FTBF) which provided a proton beam from the Fermilab Main Injector accelerator at 120 GeV, and secondary beams composed of electrons, pions, and muons of energies ranging from 4 GeV to 32 GeV. A simple schematic diagram of the experimental setup is shown in Figure 3. A small plastic scintillator of transverse dimensions 1.8 mm \times 2 mm is used as a trigger counter to initiate the read out of the data acquisition (DAQ) system and to select incident beam particles from a small geometric area, allowing us to center the beam particles on the silicon sensor. Next, we place a stack of tungsten absorbers of various thicknesses for measurements of the longitudinal profile of the electromagnetic shower. The silicon pad sensor is located within a metal box covered by copper foil, and is placed immediately downstream of the absorber plates. Finally, a Photek 240 micro-channel plate photomultiplier detector [1–4] is placed furthest downstream, and serves to provide a very precise reference timestamp. Its precision was previously measured to be less than 10 ps [3]. A photograph showing the various detector components is presented in Figure 4. A differential Cherenkov counter is located further upstream of our experimental setup and provides additional particle identification capability. More details of the experimental setup are described in our previous studies using the same experimental facility in references [1–4].

The DAQ system is based on a CAEN V1742 digitizer board [8], which provides digitized waveforms sampled at 5 GS/s. The metal box containing the silicon sensor was located on a motorized X-Y moving stage allowing us to change the location of the sensor in the plane transverse to the beam at an accuracy better than 0.1 mm. A nominal bias voltage of 500 V was applied to deplete the silicon sensor in most of the studies shown below, unless noted otherwise.

4 Test Beam Measurements and Results

Measurements were performed using the primary 120 GeV proton beam, and secondary beams provided for the FTBF. Secondary beams with energies ranging from 4 GeV/c² to 32 GeV/c² were used. Electron purity for those beams ranges between 70% at the lowest energy to about 10% at the highest energy. Stacks of tungsten plates with varying thicknesses were placed immediately upstream of the silicon device in order to measure the response along the longitudinal direction of

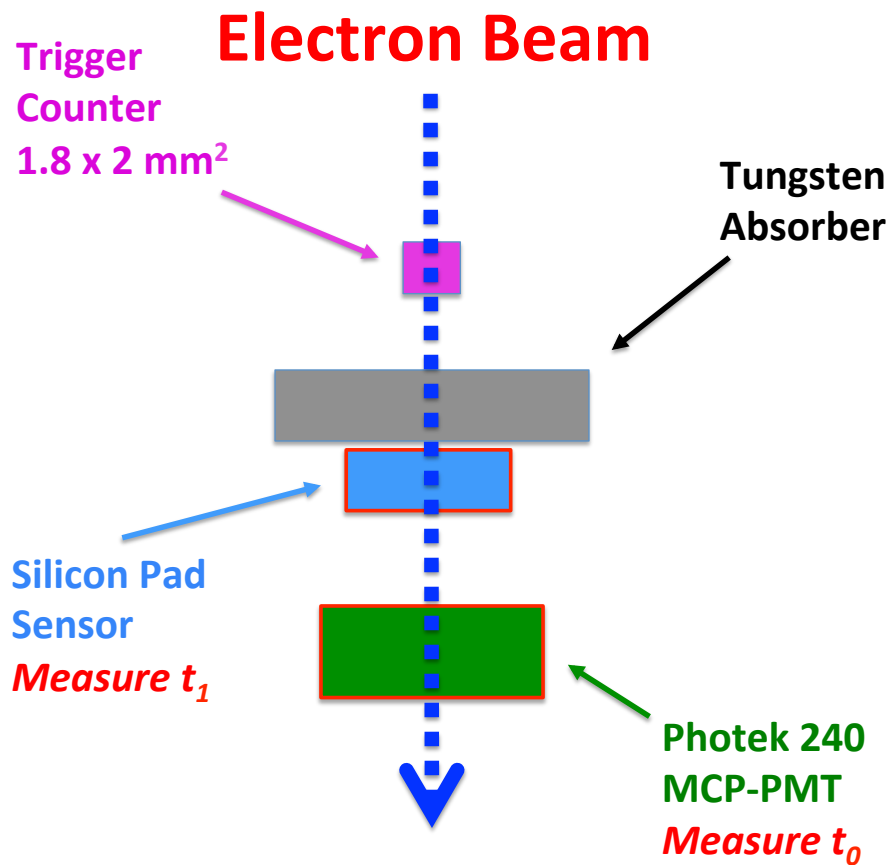


Figure 3: A schematic diagram of the test-beam setup is shown. The t_0 and t_1 are defined in Section 4.

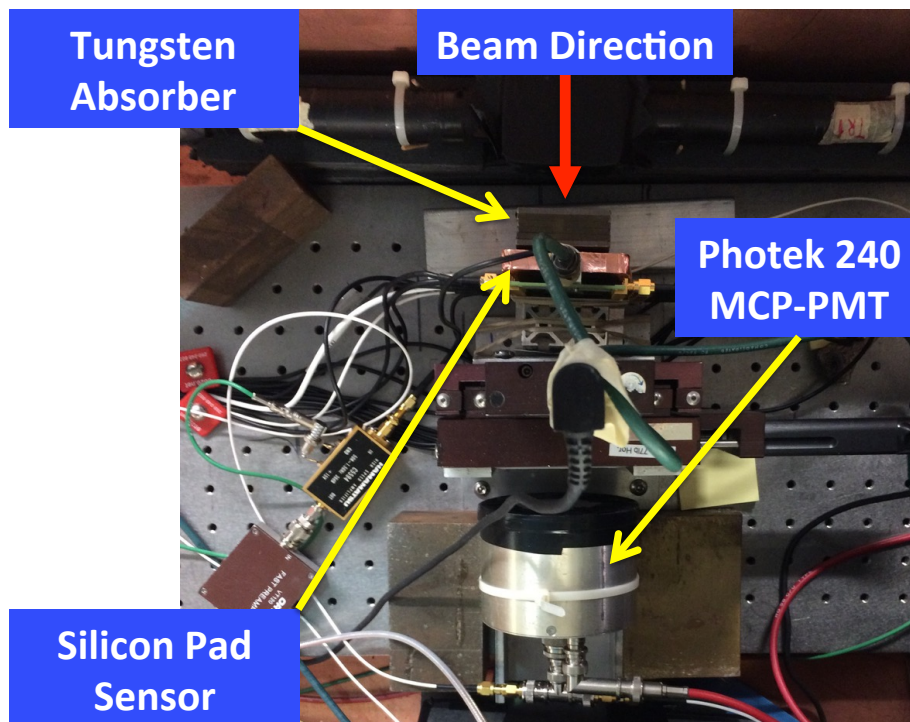


Figure 4: Test beam setup.

the electromagnetic shower. The radiation length of tungsten is 3.5 mm, and the Moliere radius is 9.3 mm. The tungsten plate size is sufficient to fully contain the shower in the transverse dimension. Signals from the silicon sensor and the Photek MCP-PMT are read out and digitized by the CAEN V1742 digitizer, and example signal waveforms are shown in Fig. 5. The signal pulse in the silicon sensor has a rise time of about 1.5 ns, and a full pulse width of around 7 ns. This rise time is consistent with a time constant of a silicon sensor coupled to a 50 Ohm amplifier.

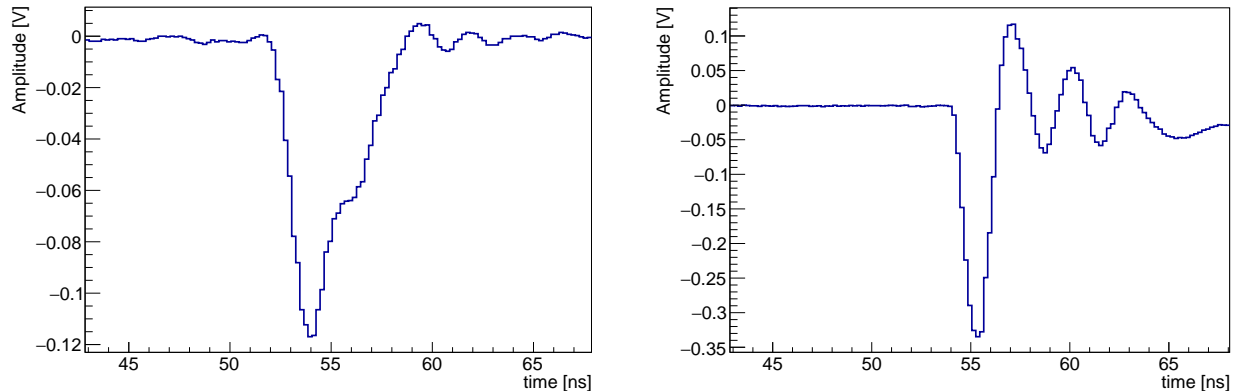


Figure 5: Examples of the signal pulse waveform for the silicon sensor (left) and the Photek MCP-PMT (right) digitized by CAEN V1742 digitizer board. The bias voltage applied to the silicon pad sensor is 500 V.

The CAEN digitizer is voltage and time calibrated using the procedure described in Ref. [9]. The total collected charge for each signal pulse is computed by integrating a 10 ns window around the peak of the pulse. The time for the reference Photek MCP-PMT detector is obtained by fitting the peak region of the pulse to a Gaussian function and the mean parameter of the Gaussian is assigned as the timestamp t_0 . The time for signals from the silicon sensor is obtained by performing a linear fit to the rising edge of the pulse and the time at which the pulse reaches 30% of the maximum amplitude is assigned as its timestamp t_1 . We measured the electronic time resolution of the CAEN V1742 digitizer as ~ 4 ps and neglected its impact on the timing measurements described below.

Electrons were identified using a combination of the gas Cherenkov counter provided by the FTBF and the signal amplitude in the Photek detector located further downstream of the silicon sensor. Electromagnetic showers induced by electrons produce significantly larger signals in the Photek MCP-PMT, while pions produce much smaller signals. After imposing the electron identification requirements the electron purity is between 80% and 90% for all beam conditions.

We begin by establishing the signal characteristics of a minimum-ionizing particle (MIP) using beams of 120 GeV protons and 8 GeV electrons with no absorbers upstream of the silicon pad sensor. To separate MIP signals from noise, we first collect data events with no beam and random trigger. The charge distribution for these noise runs is presented in Fig. 6. As expected, the charge distribution is centered at 0, and the RMS is about 2 fC.

In Figure 7, we show the response of the silicon sensor to the proton and electron beams without any absorbers upstream. We observe very similar response for these two cases, and measure an integrated charge of 4.5 fC and 5.0 fC for the proton and electron beams, respectively. The measured charge is corrected for the gain of the amplifiers and attenuators used, and hence is the output of the silicon sensor. We expect that a MIP traversing a silicon sensor of thickness $325 \mu\text{m}$ to produce roughly 35,000 electron-hole pairs, corresponding to a collected charge of about 5 fC. Thus, our measured value is in agreement with expectations. Having established the absolute scale of the response using MIPs, in our remaining studies we normalize all charge measurements to the charge integrated in the silicon sensor for one MIP, Q_{MIP} .

We study the response of the silicon sensor to electron beams of various energies after 6 radiation

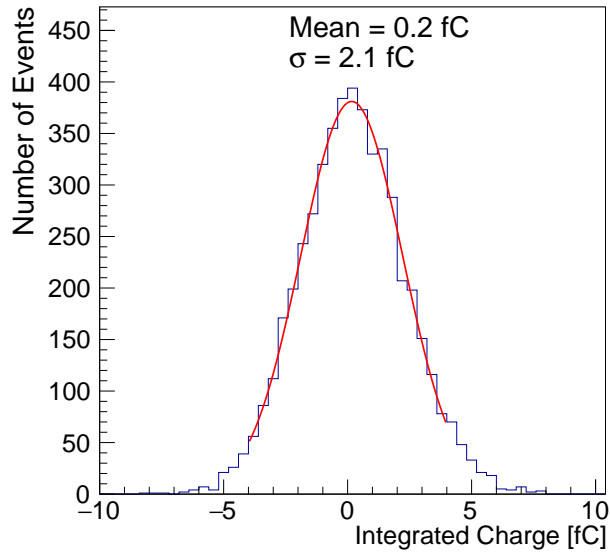


Figure 6: The distribution of charge integrated in the silicon sensor is shown for data events with no beam and random trigger.

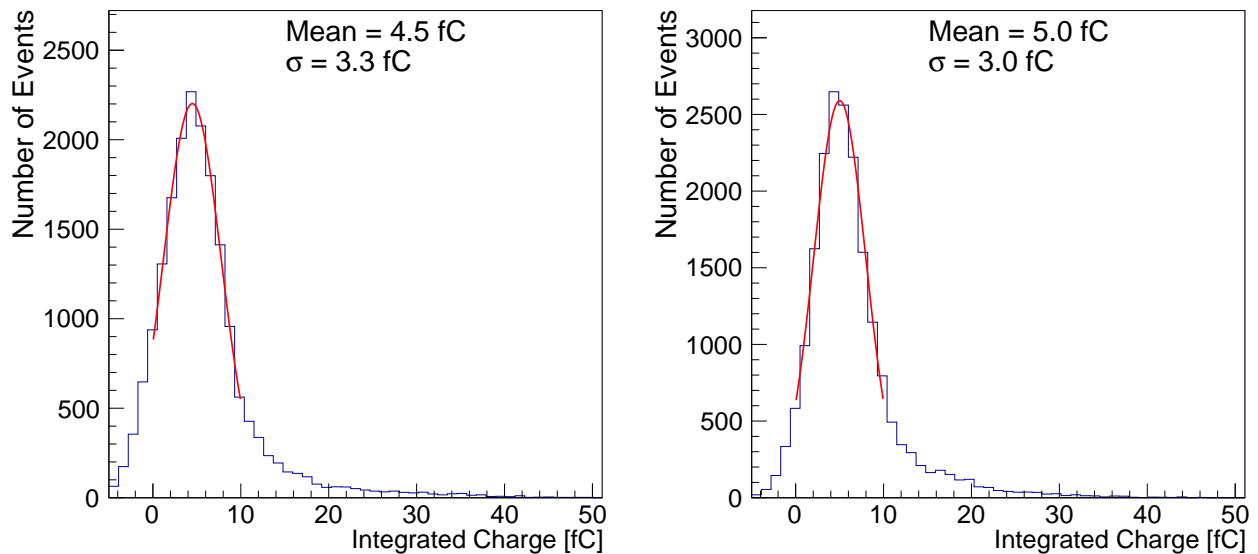


Figure 7: The distribution of charge integrated in the silicon sensor is shown for a beam of 120 GeV protons (left) and 8 GeV electrons (right) without any absorber upstream of the silicon sensor. These conditions mimic the response of the silicon sensor to a minimum-ionizing particle.

lengths (X_0) of tungsten absorber. The silicon sensor is expected to be sensitive to the number of secondary electrons produced within the electromagnetic shower, and therefore its response is expected to scale up with higher incident electron energy. In Figure 8, we show an example of the integrated charge distribution measured in the silicon sensor after 6 radiation lengths of tungsten, for runs with 32 GeV electrons. We plot the mean and RMS of these distributions as a function of incident electron beam energy in Figure 9. The uncertainties plotted show the RMS of the charge distribution. We observe a fairly linear dependence between the measured charge and the incident beam energy, for beam energies between 4 GeV and 32 GeV.

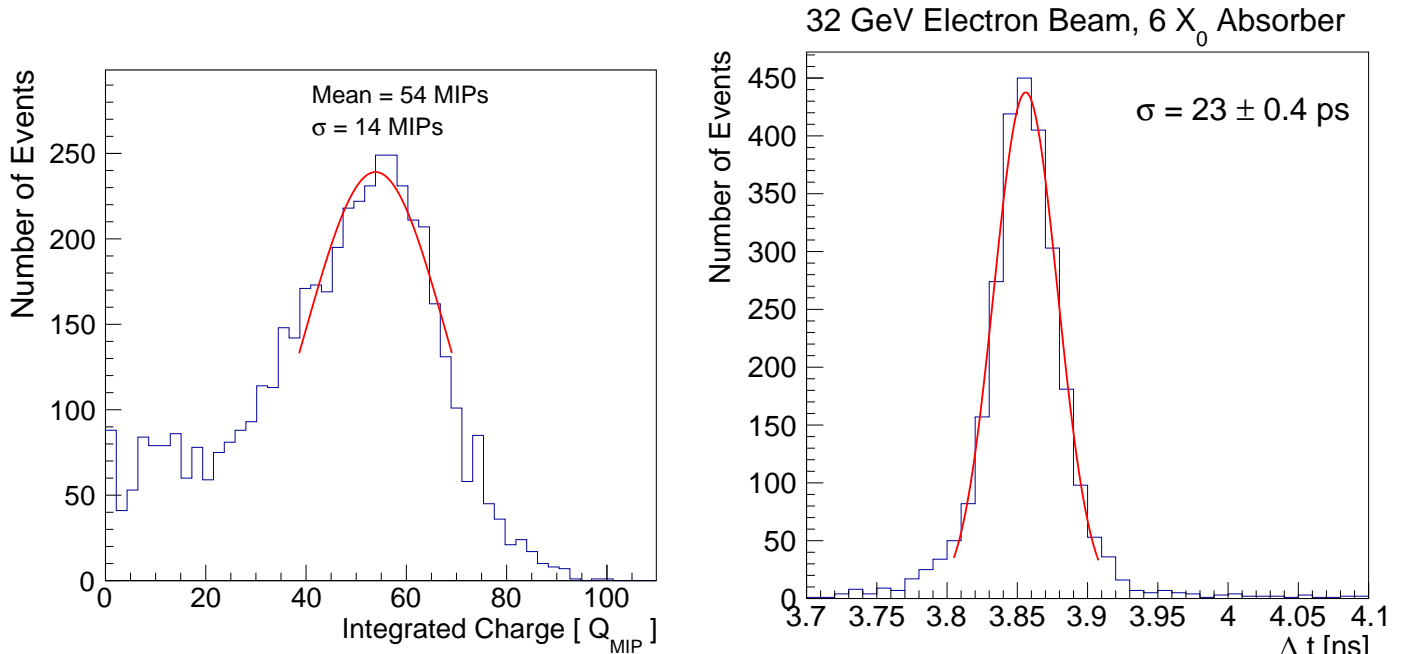


Figure 8: Left: An example of the distribution of integrated charge in the silicon sensor shown in units of charge measured for a MIP. Right: The distribution of Δt between the silicon sensor and the Photek MCP-PMT. A 32 GeV electron beam is used, and the silicon sensor is placed after 6 X_0 of tungsten absorber.

We also measure the time resolution between the silicon sensor and the Photek MCP-PMT, by measuring the standard deviation of the gaussian fit to the distribution of $\Delta t = t_0 - t_1$. We observe a systematic dependence of Δt on the total charge measured in the silicon detector, as shown in Figure 10. We perform a correction to Δt for each event using the measured charge in the silicon sensor. The correction is obtained from a second degree polynomial fit to the distribution of the Δt versus total charge collected in the silicon sensor, as shown in Figure 10. We verify that the correction flattens the dependence of the time measurement on the integrated charge, as shown on the right panel of Figure 10. An example of a corrected Δt distribution for 32 GeV electrons after 6 X_0 is shown on the right of Figure 8. Other than the electron identification requirements, no additional selection requirements on the amplitude of the signal in the silicon sensor were made. The dependence of the measured time resolution on the beam energy is shown on the right of Figure 9. We observe an improvement in the time resolution as beam energy increases, and achieve a time resolution of 23 ps for the 32 GeV electron beam.

Furthermore, we study the response and time resolution of the silicon sensor along the longitudinal direction of the shower development. We measure the integrated charge and the time resolution as a function of the absorber thickness and present the results in Figure 11. A typical longitudinal shower profile is observed, consistent with previous studies performed using a secondary emission calorimeter prototype based on MCP's [3], as well as independent studies of silicon-based calorime-

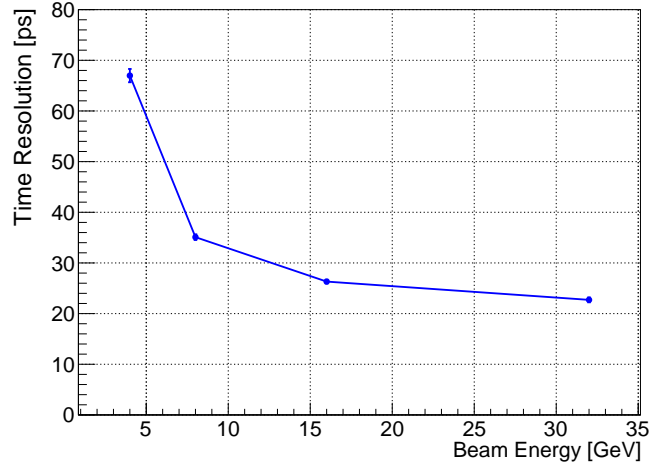
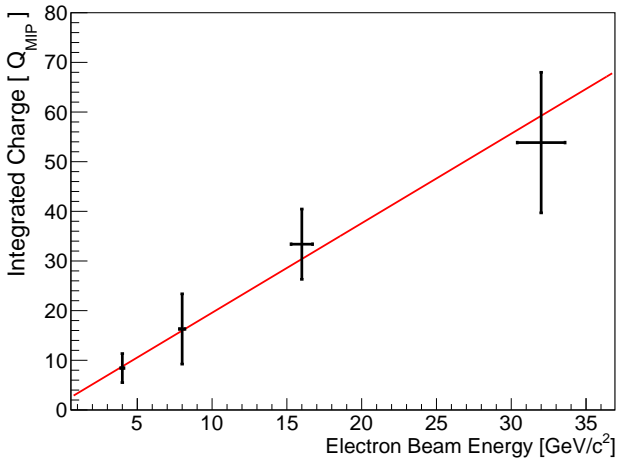


Figure 9: Left: The integrated charge in the silicon sensor expressed in units of the charge measured for a MIP is shown as a function of the electron beam energy. The uncertainty bands show the RMS of the measured charge distribution. The red line is the best fit to a linear function. Right: The measured time resolution between the silicon sensor and the Photek MCP-PMT reference is shown as a function of the electron beam energy.

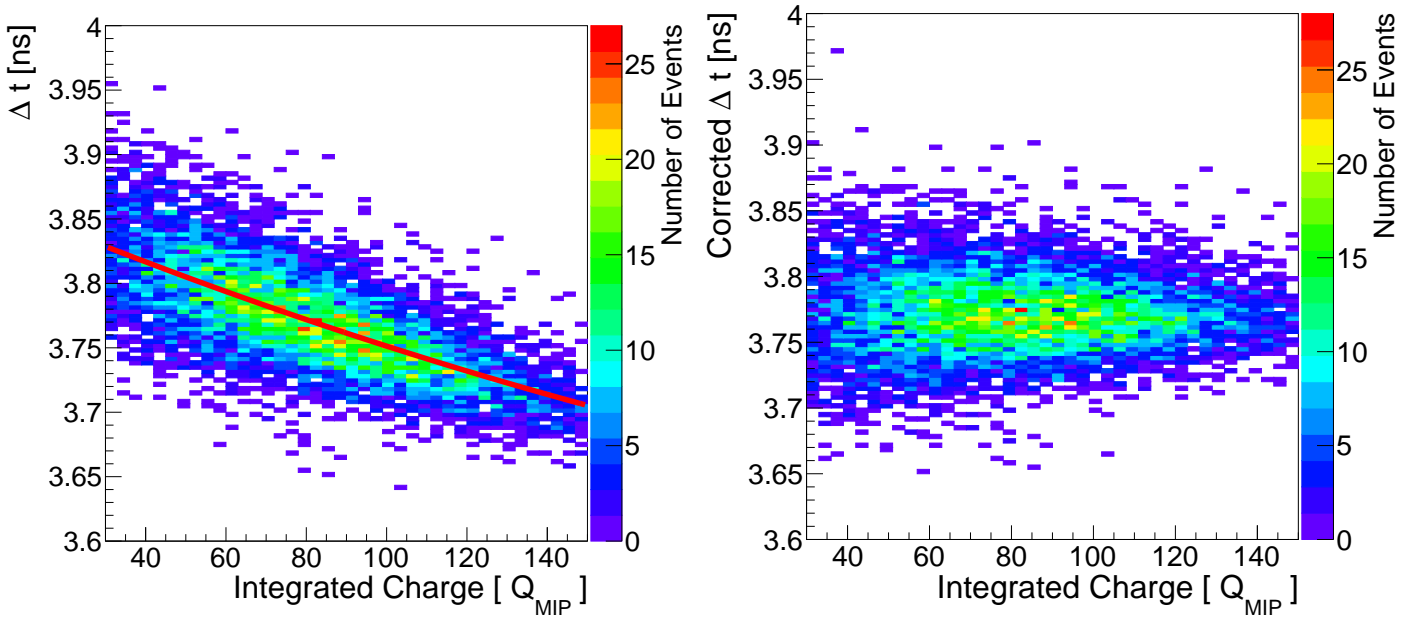


Figure 10: The dependence of Δt on the integrated charge in the silicon sensor is shown on the left. The red curve represents the fit to the profile plot of the two dimensional distribution, and is used to correct Δt for this effect. On the right, we show the corresponding two dimensional distribution after performing the correction.

ter prototypes [10]. We also observe that the time resolution improves as the shower develops towards its maximum in the longitudinal direction.

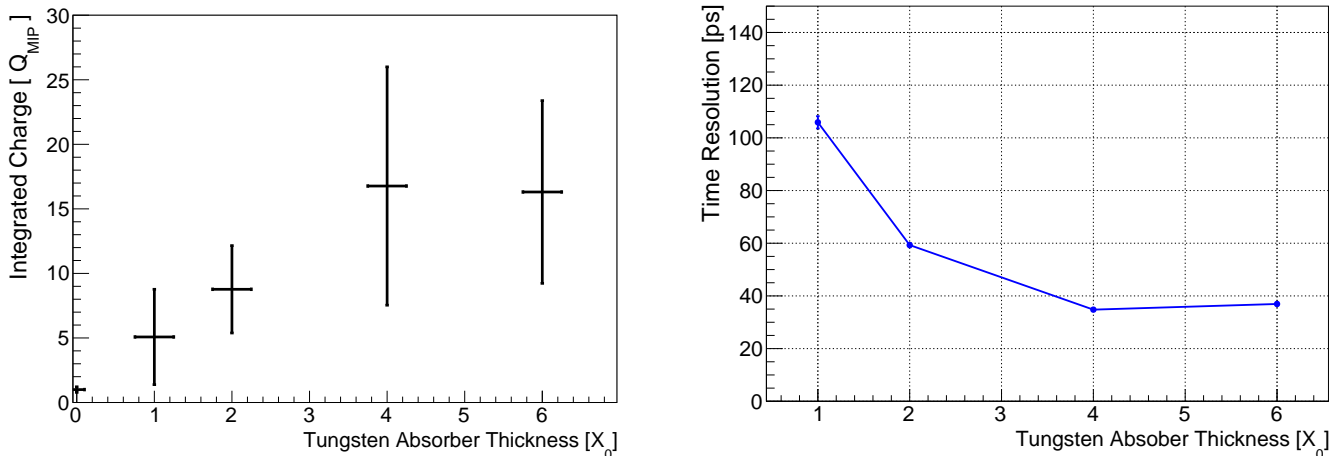


Figure 11: On the left, the integrated charge in the silicon sensor expressed in units of the charge measured for MIPs is shown as a function of the absorber (W) thickness measured in units of radiation lengths (X_0). The uncertainty bands show the RMS of the measured charge distribution. On the right, the time resolution between the silicon sensor and the Photek MCP-PMT reference is shown as a function of the absorber thickness.

Finally, we studied the dependence of the time resolution as a function of the bias voltage applied to deplete the silicon sensor. The measurements are shown in Figure 12 for 16 GeV electrons after 6 X_0 of tungsten absorber. We find that the time resolution improves as the bias voltage is increased, which is expected on the basis of increased velocity of electrons and holes in silicon at larger bias voltage.

5 Discussion

From Figures 6 and 7, we observe that the noise of the prototype system is sufficiently low to extract signals from MIPs. Comparing the RMS of the noise distribution with the mean of the MIP signal, we find a signal-to-noise ratio around 2 to 2.5. A rough estimate from Figure 7 demonstrates that the efficiency to detect 120 GeV protons and 8 GeV electrons with no absorber present is larger than 80%. Based on the measurements for MIPs, we derive signal distributions for electromagnetic showers normalized to MIP response, and observe a relatively linear response to the electron beam energy in the range from 4 GeV to 32 GeV after 6 X_0 of tungsten absorber, as shown in Figure 9. We also measure a longitudinal shower profile in Figure 11 that is consistent with similar past measurements.

Our results show that the time stamp associated with electromagnetic showers induced by electrons with energy between 20 GeV and 30 GeV can be measured with a precision better than 25 ps. Subtracting for the resolution of the reference Photek MCP-PMT detector yields a precision close to 20 ps. Moreover, we observe an improvement of the time resolution with the energy of the electron, and more generally with an increase in the signal amplitude. These measurements demonstrate that a calorimeter based on silicon sensors as the active medium can achieve intrinsic time resolution at the 20 ps level, as long as noise is kept under control. Time jitter arising from intrinsic properties of the silicon sensor is demonstrated to be well below the 20 ps level.

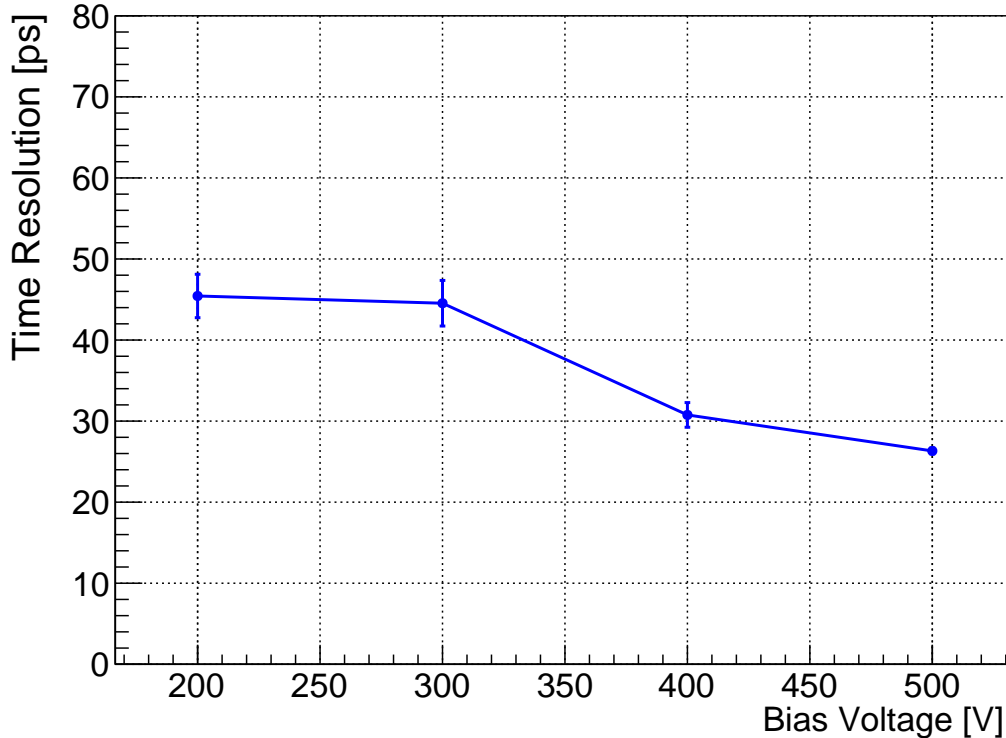


Figure 12: The time resolution between the silicon sensor and the Photek MCP-PMT reference is shown as a function of bias voltage applied on the silicon sensor.

6 Conclusion

The best time resolution of 23 ps for a silicon sensor was achieved with a 32 GeV beam and with the silicon sensor placed after 6 radiation lengths of tungsten absorber. Based on our calibration data for the response of the silicon sensor to MIPs, this measurement corresponds roughly to an average of 54 secondary particles registered from the electromagnetic shower. We observe a roughly linearly increasing response as the energy of the electron beam is increased, and we observe a longitudinal shower profile consistent with similar past measurements. This result yields further encouragement to use silicon for active layers in calorimeters, as is planned for example for the CMS Phase 2 upgrade [6], and explicitly demonstrates the opportunity to use silicon for timing measurements in future calorimeters. To continue, we plan to extend our studies to more realistic prototypes covering larger transverse and longitudinal regions of the electromagnetic shower and using multiple channels.

7 Acknowledgements

Operated by Fermi Research Alliance, LLC under Contract No. De-AC02-07CH11359 with the United States Department of Energy. We thank the FTBF personnel for very good beam conditions during our test beam time. We also appreciate the technical support of the Fermilab SiDet department for the production of high quality silicon samples.

References

- [1] D. Anderson, A. Apresyan, A. Bornheim, J. Duarte, C. Pena, A. Ronzhin, M. Spiropulu, J. Trevor, and S. Xie, “On Timing Properties of LYSO-Based Calorimeters,” *Nucl. Instrum. Meth. A*, vol. 794, pp. 7–14, 2015.
- [2] A. Ronzhin, S. Los, E. Ramberg, M. Spiropulu, A. Apresyan, S. Xie, H. Kim, and A. Zatserklyaniy, “Development of a new fast shower maximum detector based on microchannel plates photomultipliers (MCP-PMT) as an active element,” *Nucl. Instrum. Meth. A*, vol. 759, pp. 65 – 73, 2014.
- [3] A. Ronzhin, S. Los, E. Ramberg, A. Apresyan, S. Xie, M. Spiropulu, and H. Kim, “Study of the timing performance of micro-channel plate photomultiplier for use as an active layer in a shower maximum detector,” *Nucl. Instrum. Meth. A*, vol. 795, pp. 288 – 292, 2015.
- [4] A. Ronzhin, S. Los, E. Ramberg, A. Apresyan, S. Xie, M. Spiropulu, and H. Kim, “Direct tests of micro channel plates as the active element of a new shower maximum detector,” *Nucl. Instrum. Meth. A*, vol. 795, pp. 52 – 57, 2015.
- [5] L. Brianza and F. Cavallari and D. Del Re and S. Gelli and A. Ghezzi and C. Gotti and P. Govoni and C. Jorda Lopez and A. Martelli and B. Marzocchi and P. Meridiani and G. Organtini and R. Paramatti and L. Perni and S. Pigazzini and S. Rahatlou and C. Rovelli and F. Santanastasio and T. Tabarelli de Fatis and N. Trevisani, “Response of microchannel plates to single particles and to electromagnetic showers,” *Nucl. Instrum. Meth. A*, vol. 797, pp. 216 – 221, 2015.
- [6] J. Butler, D. Contardo, M. Klute, J. Mans, and L. Silvestris, “Technical Proposal for the Phase-II Upgrade of the CMS Detector,” Tech. Rep. CERN-LHCC-2015-010. LHCC-P-008, CERN, Geneva, Jun 2015.
- [7] https://www.hamamatsu.com/resources/pdf/ssd/e10_handbook_for_high_energy.pdf.
- [8] <http://www.caen.it/csite/CaenProd.jsp?parent=11&idmod=661>.
- [9] H. Kim, C.-T. Chen, N. Eclov, A. Ronzhin, P. Murat, E. Ramberg, S. Los, W. Moses, W.-S. Choong, and C.-M. Kao, “A new time calibration method for switched-capacitor-array-based waveform samplers,” *Nucl. Instrum. Meth. A*, vol. 767, pp. 67 – 74, 2014.
- [10] S. Muhuri, S. Mukhopadhyay, V. B. Chandratre, M. Sukhwani, S. Jena, S. A. Khan, T. K. Nayak, J. Saini, and R. N. Singaraju, “Test and characterization of a prototype silicon-tungsten electromagnetic calorimeter,” *Nucl. Instrum. Meth. A*, vol. 764, pp. 24 – 29, 2014.